Supplementary Materials

S1. Vehicle Dynamics

The dynamics of the vehicle on an incline with slope γ, which is a localized representation of substrate under the vehicle helps explain the acceleration's dependence on the heading θ and local tilting angle γ (Fig. S1a) in experiments. On the incline, we denote the direction along the gravity as $\|$ and the direction perpendicular to it as $\perp$ so that the acceleration from the gravity field is $a_{\perp}^{g} = 0, \sim a_{\|}^{g} = g \sin \gamma$ (Fig. S1b). Considering this incline as a localized picture of the vehicle's immediate substrate, here $\hat{\perp}$ direction stands for the $\hat{\varphi}$ and $\hat{\|}$ direction stands for the $\hat{r}$.

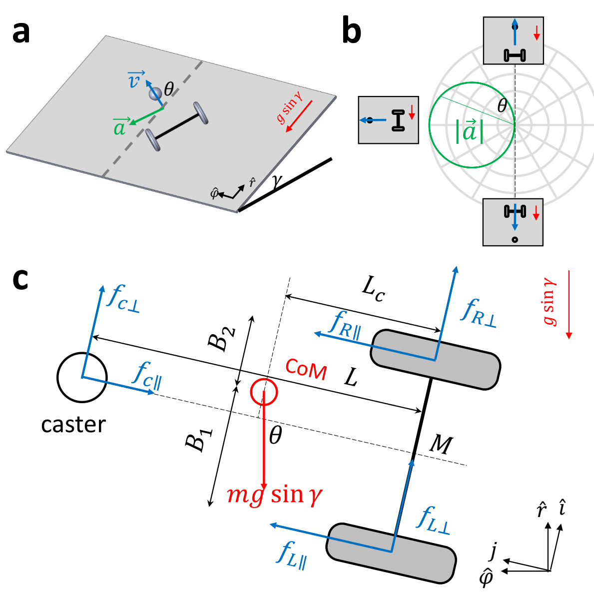

Figure S1: Vehicle dynamics of the robotic vehicle. (a) Modelling the dynamics of the vehicle on a slope with incline angle equalled to its current tilt γ. (b) The magnitude of the acceleration changes with the heading angle θ and vanishes when going along the gradient of the incline. (c) The force diagram of the vehicle.

Since the friction on the rolling caster is much smaller than the other friction forces, the vehicle rotates about the middle point of the wheel axis, M. The torque about M consists of the frictions on the two wheels and the caster, as well as the gravity component in the plane. Since the two wheels are connected to a differential drive, the torques generated by the friction parallel to the wheel $f_{L\|}, f_{R\|}$ are of same magnitude and opposite signs and therefore cancelled out. The torques generated by the friction perpendicular to the wheel are zero since the forces pass through M.

The non-zero torques left with us are the one generated by the gravity component in the plane and the friction from the caster f_c:

$$\begin{aligned}\tau &= \left(\Delta B\ \hat{i} + L_c\ \hat{j}\right) \times \\ &\quad mg\sin\gamma(-\sin\theta\ \hat{i} - \cos\theta\ \hat{j}) + L\ \hat{j} \times f_{c\perp}\ \hat{i} \qquad (1)\\ &= \left(mg\sin\gamma\left(-\Delta B\cos\theta + L_c\sin\theta\right) - f_{c\perp}L\right)\hat{k} \qquad (2)\end{aligned}$$

where $\Delta B \equiv \frac{1}{2}(B_2 - B_1)$.

The moment of inertia of the vehicle with respect to M is $I = I_{\text{vehicle}} + m(L^2 + \Delta B^2)$ where we approximate $I_{\text{vehicle}} = \frac{1}{2}mR_v^2$ with R_v being the radius of the vehicle since the mass distribution is quite homogeneous. Therefore the magnitude of the angular acceleration ($\beta = \tau \cdot \hat{k}/I$) and the acceleration of the center of mass on the incline is

$$\begin{aligned}a_{\text{incline}} &= \left|L_c\ \hat{j} + \Delta B\ \hat{i}\right| \cdot \beta \qquad (3)\\ &\approx L_c \cdot \frac{\tau \cdot \hat{k}}{I} \qquad (4)\\ &= \frac{mg\sin\gamma(L_c\sin\theta - \Delta B\cos\theta) - f_c L}{\frac{1}{2}mR_v^2 + mL_c^2 + m\Delta B^2} L_c \qquad (5)\end{aligned}$$

For the ideal case that the center of mass is not biased to the left or right so that $B_1 = B_2$, the acceleration is

$$\begin{aligned}a_{\text{incline}} &= \frac{mgL_c\sin\gamma\sin\theta - f_c L}{\frac{1}{2}mR_v^2 + mL_c^2} L_c \\ &= \frac{L_c^2}{\frac{1}{2}R_v^2 + L_c^2} g\sin\gamma\sin\theta - \frac{f_c L}{\frac{1}{2}mR_v^2 + mL_c^2} \qquad (6)\end{aligned}$$

When $\theta = \pi/2$ and f_c being very small since this is a rolling friction, the acceleration projected onto the horizontal plane is

$$\begin{aligned} a(\theta = \pi/2) &= a_{\text{incline}}(\theta = \pi/2)\cos\gamma \\ &\approx \frac{L_c^2}{\frac{1}{2}R_v^2 + L_c^2} g\sin\gamma\cos\gamma \end{aligned} \tag{7}$$

The actual numbers in the experiment $R_v = 5$ cm, $L_c \approx 1$ cm give the theoretical prediction

$$a_{\text{theo}}(\theta = \pi/2) \approx 0.074\ g\sin\gamma\cos\gamma \tag{8}$$

which is quite close to the experimental measurement

$$a_{\text{expt}}(\theta = \pi/2) = (0.073 \pm 0.001)\ g\sin\gamma\cos\gamma \tag{9}$$

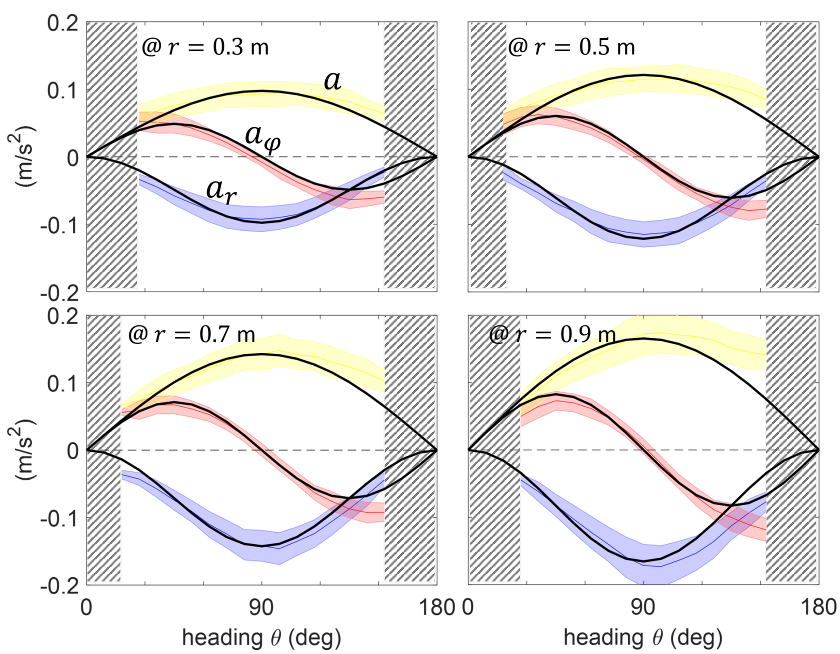

Figure S2: Acceleration at different radii. The shading colored in yellow, red and blue are the magnitude a, and the azimuthal, radial components a_φ, a_r of the acceleration respectively. The solid lines and shading in the figures denote the mean and standard deviation over 238 experiments. The black lines are the theory $a = k(r)\cdot\sin\theta$, $a_r = -a\sin\theta$, and $a_\varphi = a\cos\theta$ where $k(r)$ takes the mean value shown in Fig.3c in the main text.

In reality, there is always a small bias between B_1 and B_2, this small correction from the CoM (center of mass) offset that breaks the symmetry of acceleration with respect to the heading gives the attraction to the circular orbit and will is discussed in Section S3.

This bias is

$$a_{\text{bias}} = -g \sin\gamma \cos\theta \, \frac{L_c \Delta B}{\frac{1}{2}R^2 + L_c^2 + \Delta B^2} \tag{10}$$

where ΔB can be measured by weighing the normal force on the left and right wheels and given by

$$\Delta B = \frac{L_w}{2} \frac{N_R - N_L}{N_R + N_L} \tag{11}$$

where N_L, N_R are the normal forces on the two wheels and $L_w = 6$ cm. For an imbalance of $(N_R - N_L)/(N_R + N_L) \approx 20$ % measured from experiment, it can be inferred that $\Delta B \approx 0.6$ cm. Thus, the maximum bias ($\theta = 0°, 180°$) when driving on a typical local slope of $\gamma = 10°$ is $a_{\text{bias}} = 0.074$ m/s^2, which is about 40 % of the maximum magnitude of the acceleration in the system. Fig.S3 shows how this bias causes the slight dependence on θ.

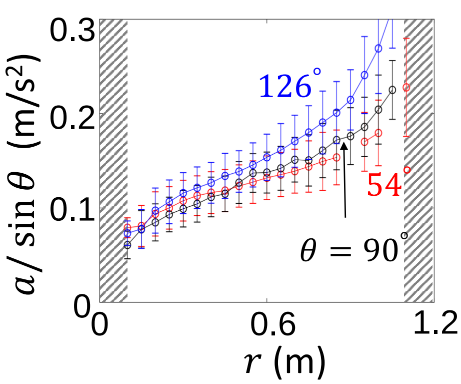

Figure S3: Plots of k as a function of r for various values of θ using $a/\sin\theta$. The gray shaded regions refer to regions which are forbidden due to steric exclusion.

S2. Transient Dynamics of a Vehicle with Slight Chirality

S2.1 Result

The transient behavior of some trajectories that decay into circular orbits is caused by the slight asymmetry in the mechanical structure that the center of mass (CoM) deviates slightly from the center-line. As shown in Section S1, the acceleration magnitude $|a|$ for a vehicle with slight asymmetry with respect to the heading is given by

$$|a| = k(r) \cdot (\sin\theta + \epsilon \cdot \cos\theta) \tag{12}$$

where $\epsilon = -\frac{\Delta B}{L_c}$ increases with the CoM's deviation from the center-line being ΔB.

This leads to the polar equation of the trajectory

$$\begin{aligned} r_{,\varphi\varphi} = & \frac{2r_{,\varphi}^2}{r} + r - \tilde{k}(r) \cdot (r^2 + r_{,\varphi}^2) \\ & - \epsilon \cdot \tilde{k}(r) \cdot (r_{,\varphi} r + \frac{r_{,\varphi}^3}{r}) \end{aligned} \tag{13}$$

where $\tilde{k} \equiv k/v^2$. Detailed derivation can be found in S2.2.

Let $r = r_c + \rho$ where ρ is the perturbation and r_c is the radius of the circular orbit that $k(r_c) = v^2/r_c$. After discarding the $O(\rho^2)$ terms, the differential equation is reduced to

$$\rho_{,\varphi\varphi} = -(1 + r_c k_c'/k_c)\rho - \epsilon\rho_{,\varphi} \tag{14}$$

where $k_c \equiv k(r_c), k_c' \equiv k'(r_c)$.

The solution to this damped oscillator gives the solution as

$$\rho(\varphi) = \rho(0)\ \cos\left(\sqrt{1 + r_c k_c'/k_c - (\epsilon/2)^2}\varphi\right)\ e^{-\epsilon\varphi/2} \tag{15}$$

with an exponentially decaying envelope with a half-life $(2\log 2)/\epsilon$ that degrades with the bias; that is, the larger the imperfection is, the faster the trajectory is attracted a circular orbit.

On the other hand, when the vehicle has an acceleration bias towards the orbit direction, ϵ will be negative, then ρ will expand and leads the orbit to either crash to the center or escape from the membrane. From this example with clockwise trajectory, we see that the orbit is attracted to a circular orbit when $\epsilon \propto (B_2 - B_1) > 0$, that is when the CoM is biased to the left wheel. The data listed in Section S1 shows an estimate $\epsilon \approx 0.5$, indicating a half life of $(2\log 2)/0.5 \approx 3$. This qualitatively matches with our experimental observation of the transient orbits when the vehicle tested on a leveled ground does not drive sufficiently straight. We posit the quantitative difference may come from the inaccuracy of the ΔB and L_c estimate.

In summary, a counterclockwise (clockwise) orbit will get attracted to a circular orbit when the CoM is biased to the right (left) while the eccentricity increases to escape or crash when the CoM is biased to the left (right).

2.2 Derivation

We consider a slightly simpler case where the membrane is rather flat that $\Psi^2 = 1 + (\partial z/\partial r)^2 \approx 1$. The acceleration components in radial and azimuthal directions are given by Eqs.1, 2 in the main text as

$$\begin{cases} r\ddot{\varphi} + 2\dot{r}\dot{\varphi} = a_\varphi = f & \text{(16a)} \\ \ddot{r} - r\dot{\varphi}^2 = a_r = -f \cdot \tan\theta & \text{(16b)} \end{cases}$$

where $f = k(r) \cdot (\sin\theta + \epsilon\cos\theta)\cos\theta$ for a vehicle with bias ϵ.

The definition of the heading θ gives

$$\tan\theta \equiv \frac{v_\varphi}{v_r} = \frac{r\dot{\varphi}}{\dot{r}}. \tag{17}$$

Using $\dot{\varphi} = \dot{r}\tan\theta/r$, we get the time derivatives of azimuth φ as

$$\dot{\varphi} = \frac{\dot{r}\tan\theta}{r}, \qquad \ddot{\varphi} = \frac{\ddot{r}\tan\theta}{r} + \frac{\dot{r}\dot{\theta}\sec^2\theta}{r} - \frac{\dot{r}^2\tan\theta}{r^2}. \tag{18}$$

Substitute the $\dot{\varphi}$ and $\ddot{\varphi}$ in (16) with (18) and eliminate $\ddot{r}$ by (16a)-(16b)$\cdot\tan\theta$, we have

$$\dot{r}\dot{\theta} + \frac{\dot{r}^2}{r}\tan\theta = f. \tag{19}$$

Consider the radial speed as the velocity's projection on the radial direction $\dot{r} = v{\cdot}\cos\theta$, we arrive at the vector field description:

$$\begin{cases} \dot{r} = v \cdot \cos\theta & \text{(20a)} \\ \dot{\theta} = \dfrac{f(r,\theta)}{v\cdot\cos\theta} - \dfrac{v\cdot\sin\theta}{r}. & \text{(20b)} \end{cases}$$

Plug in $f = k(r)\cdot(\sin\theta + \epsilon\cos\theta)\cos\theta$, we have

$$\begin{cases} \dot{r} = v \cdot \cos\theta & \text{(21a)} \\ \dot{\theta} = (k/v - v/r)\sin\theta + (k/v)\epsilon\cos\theta. & \text{(21b)} \end{cases}$$

Divide (21a) by (21b), we have

$$\frac{dr}{d\theta} = \frac{v\cdot\cos\theta}{(k(r)/v - v/r + (k(r)/v)\epsilon\cos\theta)\cdot\sin\theta}. \tag{22}$$

As we want r to be a function of the azimuth φ, we convert all θ to φ. We use the definition of heading again $\tan\theta = r\dot{\varphi}/\dot{r} = (rd\varphi/dt)/(dr/dt) = rd\varphi/dr = r/r_{,\varphi}$, $\sin\theta = r/\sqrt{r^2 + r_{,\varphi}^2}$, and $\cos\theta = r_{,\varphi}/\sqrt{r^2 + r_{,\varphi}^2}$. The left hand side of (22) can thus be converted to

$$LHS = \frac{dr}{d\theta} = \frac{1}{\theta_r} = \frac{1}{\frac{d(\arctan(r/r_{,\varphi}))}{d(r/r_{,\varphi})}\cdot\frac{d(r/r_{,\varphi})}{dr}} = \frac{1}{[1 + (r/r_{,\varphi})^2]^{-1}\cdot\left[\frac{1}{r_{,\varphi}} - \frac{r\cdot r_{,\varphi\varphi}}{r_{,\varphi}^3}\right]} \tag{23}$$

The right hand side can be converted to

$$RHS = \frac{r_{,\varphi}}{(\tilde{k} - 1/r)\cdot r + \epsilon\tilde{k}r_{,\varphi}}. \tag{24}$$

where $\tilde{k}(r) \equiv k(r)/v^2$.

Equate the LHS (23) and the RHS (24), we finally arrive at

$$r_{,\varphi\varphi} = \frac{2r_{,\varphi}^2}{r} + r - \tilde{k}(r)\cdot(r^2 + r_{,\varphi}^2) - \epsilon\cdot\tilde{k}(r)\cdot(r_{,\varphi}r + \frac{r_{,\varphi}^3}{r}). \tag{25}$$

S3. Trajectory resulting from active vehicle deviates from spatial-only geodesics

To measure the spatial-only trajectory, we let the left and right wheel speed of the vehicle be the same. The spatial-only trajectory (blue) enabled by the same left and right wheel speeds is much straighter than that of an active vehicle responding the local gradient (red).

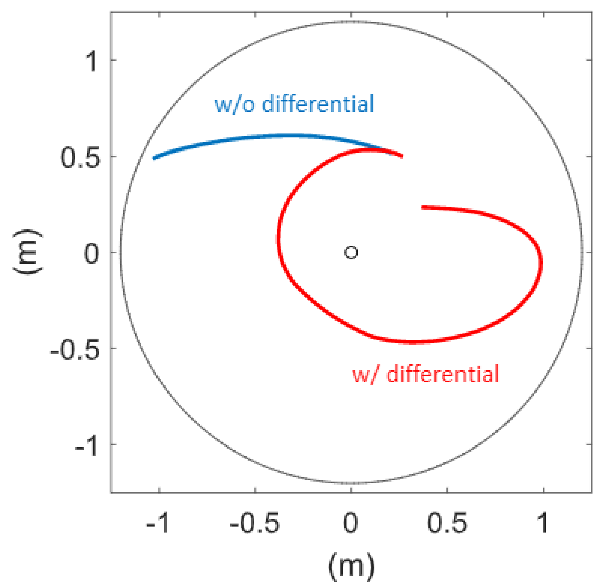

Figure S4: Comparison of the trajectories of the vehicle on the membrane when differential mechanism is applied and disabled. To disable the differential mechanism so that the two wheels are rigidly connected, the gears in the differential are glued.

S4. Conserved quantities

The metric $ds^2 = -\alpha^2 dt^2 + \Phi^2(\Psi^2 dr^2 + r^2 d\varphi^2)$ gives

$$-1 = -\alpha^2 \mathring{t}^2 + \Phi^2(\Psi^2 \mathring{r}^2 + r^2 \mathring{\varphi}^2) \tag{26}$$

where $dq/d\lambda \equiv \mathring{q}$ and we specify the affine parameter λ to be s. To convert the $\mathring{q}$ to $\dot{q}$, we use $\mathring{t} = E/\alpha^2$ and $\mathring{\varphi} = L/\Phi^2 r^2$ from the conserved quantities in geodesic equations (see 'Robophysical modeling of spacetime dynamics (arXiv:2202.04835)' for details). Using $\mathring{t} = E/\alpha^2$ again in $\mathring{r}$, we have $\mathring{r} = dr/d\lambda = (dr/dt)(dt/d\lambda) = \dot{r}\mathring{t} = (E/\alpha^2)\dot{r}$. Plug these into Eq.26, we have

$$-1 = -\frac{E^2}{\alpha^2} + \Phi^2\Psi^2 \frac{E^2 \dot{r}^2}{\alpha^4} + \frac{L^2}{\Phi^2 r^2} \tag{27}$$

Multiply both sides with $-\alpha^2/E^2$ and rearrange the terms, we arrive at

$$1 = \frac{\Phi^2}{\alpha^2}\Psi^2 \dot{r}^2 + \frac{1}{r^2}\frac{\alpha^2}{\Phi^2}\frac{L^2}{E^2} + \frac{\alpha^2}{E^2} \tag{28}$$

which leads to Eq.4 in the main text.

To show the maximum of ℓ is obtained at r_0, we plug the derived metric into Eq.**??**,**??**,

$$\ell \equiv \frac{L}{E} \quad = \quad e^{-K(r_0)/v^2} r_0 \cdot v \tag{29}$$

The maximum of ℓ is obtained at r_0 that

$$\frac{\partial \ell}{\partial r_0} \quad = \quad e^{-K(r_0)/v^2} \left(1 - \frac{r_0 k(r_0)}{v^2}\right) = 0, \tag{30}$$

showing r_0 coincides with the circular orbit radius r_c such that $k(r_c) = v^2/r_c$.

S5. Generalization from axi-symmetric substrate to general substrate

We construct the general model by viewing the terrain gradient in the axi-symmetric case as an arbitrary terrain gradient. The following table shows the comparison between the special case with axi-symmetry and the general case.

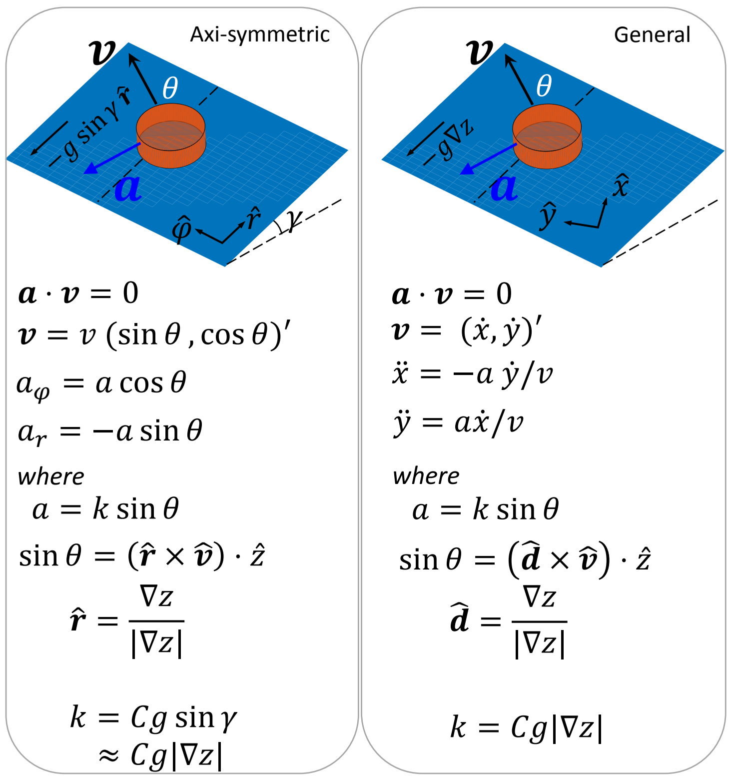

Figure S5: Generalization of the vehicle dynamics on an arbitrary terrain.

We construct the general dynamics by making analogy such that the axi-symmetric case is a special case of the general case. The analogies can be found in Fig.S5.

If we plug the generalized direction and magnitude into the acceleration components, we get

$$
\begin{aligned}
\ddot{x} &= -a\ \frac{\dot{y}}{v} && (31)\\
&= k\sin\theta\ \frac{\dot{y}}{v} && (32)\\
&= k(\hat{\boldsymbol{d}}\times\hat{\boldsymbol{v}})\cdot\hat{z}\ \frac{\dot{y}}{v} && (33)\\
&= Cg|\nabla z|\left(\frac{\nabla z}{|\nabla z|}\times\hat{\boldsymbol{v}}\right)\cdot\hat{z}\ \frac{\dot{y}}{v} && (34)\\
&= Cg(\nabla z\times\frac{\boldsymbol{v}}{v})\cdot\hat{z}\ \frac{\dot{y}}{v} && (35)\\
&= \frac{Cg}{v^2}(z_{,x}\dot{y}-z_{,y}\dot{x})\dot{y} && (36)\\
&= C\,g\,\dot{y}\,(d_x\dot{y}-d_y\dot{x})/v^2 && (37)
\end{aligned}
$$

Similarly, we have $\ddot{y} = -C\,g\,\dot{x}\,(d_x\dot{y}-d_y\dot{x})/v^2$.

In both cases, the acceleration magnitude vanishes when the velocity us along the radial (gradient) direction and the acceleration direction is perpendicular to the velocity.

S6. Membrane Measurement

S6.1 Membrane constant

To model the membrane deformation, we consider a free circular membrane with radius R only deformed by its self weight and pressed by a cap in the center with depth D and cap radius $R_0 < R$. When the load from self weight is uniform, the height of the membrane z follows

$$\Delta Z = \lambda^{-1} \tag{38}$$

where λ absorbed the elasticity and the mass density.

Applying the axi-symmetry ($\partial Z/\partial\varphi = 0$) and boundary conditions $Z(R) = 0, Z(R_0) = -D$ for a membrane without a load such as the robotic vehicle, the general solution to a membrane deformed by only self weight is

$$Z(r) = \frac{1}{4\lambda}r^2 + C_1 \log r + C_2 \tag{39}$$

where

$$C_1 = \frac{D - \frac{1}{4\lambda}(R^2 - R_0^2)}{\log{(R/R_0)}}, \tag{40}$$

$$C_2 = \frac{\frac{1}{4\lambda}(R^2 \log R_0 - R_0^2 \log R) - D \log R}{\log{(R/R_0)}} \tag{41}$$

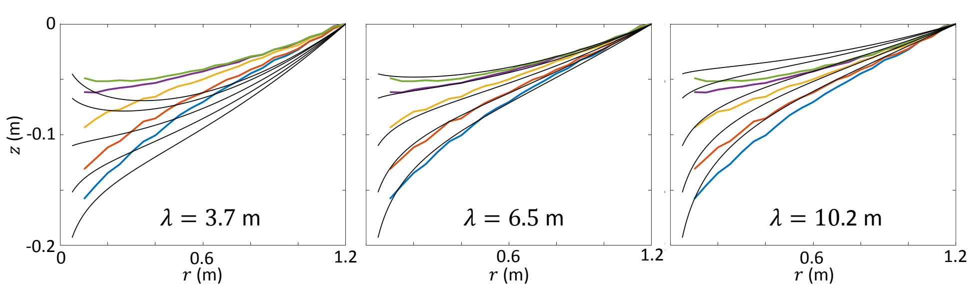

Figure S6: Membrane constant measurement: The black lines show the radial profiles of the free membrane from Poisson equation Eq.39. The colored lines show the measurement from experiments.

We measured the cross sections of the membrane with various central depressions D's and compare them with solution Eq.39 for various λ. The value of λ is chosen such that the solutions match with experiments the best. In our setup, λ is measured to be 6.5 m (Fig.S6).

S6.2 Membrane isotropy

Ideally, the height of the membrane at a particular radius should be the same for any azimuthal angle in terms of the axi-symmetry. To understand how the membrane deviates from the ideal, the variation of this height is evaluated with the data taken from the Optitrack cameras for three different central depressions. The variation is found to be smaller than 5% of the central depression.

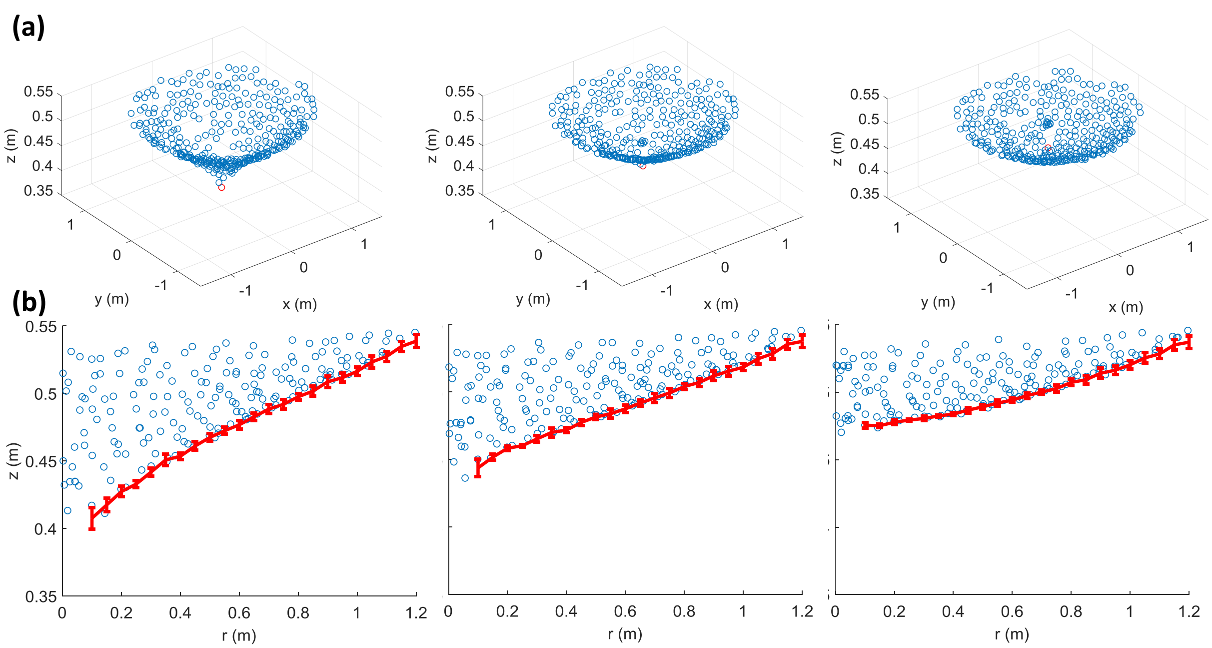

Figure S7: Shapes of the membrane with different central depressions. (a) The perspective views of the membrane profile measured from the optical tracking system. (b) The red curves show the heights averaged over the azimuthal angles.

S7. Analytic solution to the membrane

As shown in the previous section, the deformation of the membrane by its self weight can be well characterized by $\Delta Z = \lambda^{-1}$. To model the additional load from the vehicles besides the weight of the membrane itself, we evaluate the area density of vehicle and scaled it by that of the membrane so that $\Delta Z = \lambda^{-1}(1 + \tilde{P})$ with $\tilde{P} = \sigma_v/\sigma$ where σ_v and σ are the density of the vehicle ($\approx 20,000$ g/m^2) and the membrane (137 g/m^2) respectively. For simplicity, we assume the load is a uniform distribution on a disc centered at the ith vehicle's position $\mathbf{r}_i$ and with the radius of the vehicle R_v so that $\sigma_{v,i} = \frac{m_i}{\pi R_v^2} 1(\mathbf{r} \in \Omega_i)$ and $\sigma_v = \sum_i \sigma_{v,i}$ where $\Omega_i = \{\mathbf{r} : |\mathbf{r} - \mathbf{r}_i| < R_v\}$.

To solve the Poisson equation, we integrate the Green function $G(\mathbf{r}, \mathbf{s})$ of Poisson equation with the source.

$$
\begin{aligned}
\lambda Z(\mathbf{r}) &= \int G(\mathbf{r}, \mathbf{s})(1 + \tilde{P}(\mathbf{s}))d\mathbf{s}^2 && (42) \\
&= \int G(\mathbf{r}, \mathbf{s})d\mathbf{s}^2 + \frac{1}{\sigma}\sum_i \int_{\Omega_i} G(\mathbf{r}, \mathbf{s})\sigma_{v,i}(\mathbf{s})d\mathbf{s}^2 && (43) \\
&\equiv I_1 + I_2 && (44)
\end{aligned}
$$

where the Green function on a disc with radius R is

$$
\begin{aligned}
G(\mathbf{r}, \mathbf{s}) &= \frac{1}{2\pi}\log|\mathbf{r} - \mathbf{s}| \\
&- \frac{1}{2\pi}\log\left(\frac{|\mathbf{s}|}{R} \cdot \left|\mathbf{r} - R^2\frac{\mathbf{s}}{|\mathbf{s}|^2}\right|\right) && (45) \\
G(\mathbf{r}, \mathbf{0}) &= \frac{1}{2\pi}\log|\mathbf{r}| - \frac{1}{2\pi}\log R && (46)
\end{aligned}
$$

Let us consider a field point that is not covered by the vehicles $\mathbf{r} \notin \cup_i \Omega_i$. I_1 is the solution to the case with uniform load that $I_1 = \frac{1}{4}(|\mathbf{r}|^2 - R^2)$. For I_2, the source is effectively a point source since the field point is outside the source, so

$$\begin{aligned} I_2 &= \frac{1}{\sigma}\sum_i \int_{\Omega_i} G(\mathbf{r},\mathbf{s})\frac{m_i}{\pi R_v^2}\pi R_v^2 \delta(\mathbf{s}-\mathbf{r}_i) d\mathbf{s}^2 && (47) \\ &= \frac{1}{\sigma}\sum_i m_i G(\mathbf{r},\mathbf{r}_i) && (48) \end{aligned}$$

Up till so far, we have solved the shape of the membrane $Z(\mathbf{r})$. Next, we evaluate the height of the ith vehicle. Since the vehicle is not a point object, we average the membrane height Z on the rim of the vehicle to approximate the height of the vehicle z_i.

$$\begin{aligned} z_i &= \langle Z \rangle_{\partial\Omega_i} && (49) \\ \lambda z_i &= \langle I_1 + I_2 \rangle = \langle I_1 \rangle + \langle I_2 \rangle && (50) \end{aligned}$$

$\langle I_1 \rangle$ is contributed by the self weight of the entire membrane so that we approximate it by just the value at the center of the vehicle $\mathbf{r}_i$: $\langle I_1 \rangle = \frac{1}{4}(|\mathbf{r}_i|^2 - R^2)$.

For $\langle I_2 \rangle$, there are two different types of contributions. The first ones are the patches of domain from the vehicles other than the ith vehicle, the one of concern that contribute as far field. The second type is the contribution from the load of vehicle i itself.

For the first type, we still use the point source approximation:

$$\langle I_{2,j\neq i} \rangle = \frac{m_j}{\sigma} G(\mathbf{r}_i, \mathbf{r}_j) \quad (51)$$

For the second type:

$$\begin{aligned} \langle I_{2,i} \rangle &= \frac{m_i}{\sigma}\langle G(\mathbf{r},\mathbf{r}_i)\rangle_{\mathbf{r}\in\Omega_i} && (52) \\ &= \frac{m_i}{2\pi\sigma}\left(\langle \log|\mathbf{r}-\mathbf{r}_i| \rangle - \left\langle \log\left(\frac{|\mathbf{r}_i|}{R} \cdot \left| \mathbf{r} - R^2 \frac{\mathbf{r}_i}{|\mathbf{r}_i|^2} \right| \right) \right\rangle \right) \\ &= \frac{m_i}{2\pi\sigma}\left(\log R_v - \log\left(\frac{|\mathbf{r}_i|}{R} \cdot \left| \mathbf{r}_i - R^2 \frac{\mathbf{r}_i}{|\mathbf{r}_i|^2} \right| \right) \right) \\ &= \frac{m_i}{2\pi\sigma} \log\left(\frac{R_v R}{R^2 - |\mathbf{r}_i|^2} \right) && (53) \end{aligned}$$

Piecing all these terms together, we arrive at the z position of the ith vehicle is

$$\begin{aligned} 2\pi\lambda z_i &= \frac{\pi}{2}(|\mathbf{r}_i|^2 - R^2) + \frac{m_i}{\sigma}\log\left(\frac{R_v R}{R^2 - |\mathbf{r}_i|^2}\right) \\ &+ \frac{1}{\sigma}\sum_{j\neq i} m_j\left(\log\frac{|\mathbf{r}_i - \mathbf{r}_j|}{|\mathbf{r}_i - \mathbf{r}'_j|} - \log\frac{|\mathbf{r}_j|}{R}\right) \end{aligned} \tag{54}$$

where $\mathbf{r}' = (R/|\mathbf{r}|)^2\mathbf{r}$ is conventionally regarded as the position of the image charge. $\mathbf{r}_j$'s are the positions of the other vehicles.

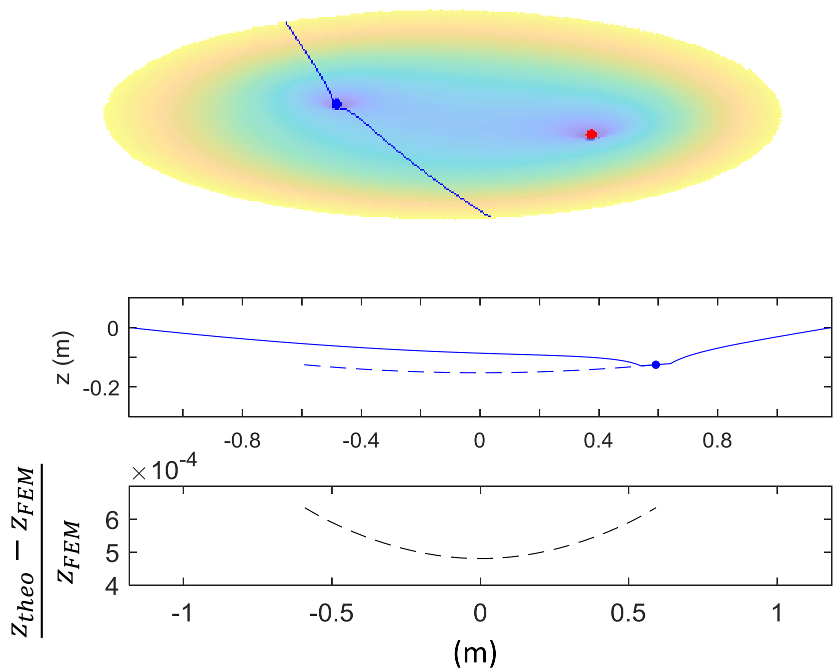

Figure S8: Numerical verification of the analytical solution: We show a test with the blue vehicle put at different y positions while the x position is fixed (0.2 m). The solid blue line shows the membrane shape and the dotted line shows the vertical position of the vehicle z when placed at different positions. The bottom panel shows the relative error of z between the analytical (Eq.54) and numerical (FEM) solution.

Despite the fact that some approximations are made, the analytical solution matches with the numerical result (FEM) with a relative error smaller than 10^{-3} (Fig.S8).

S8. Dynamics of two vehicles with the same mass

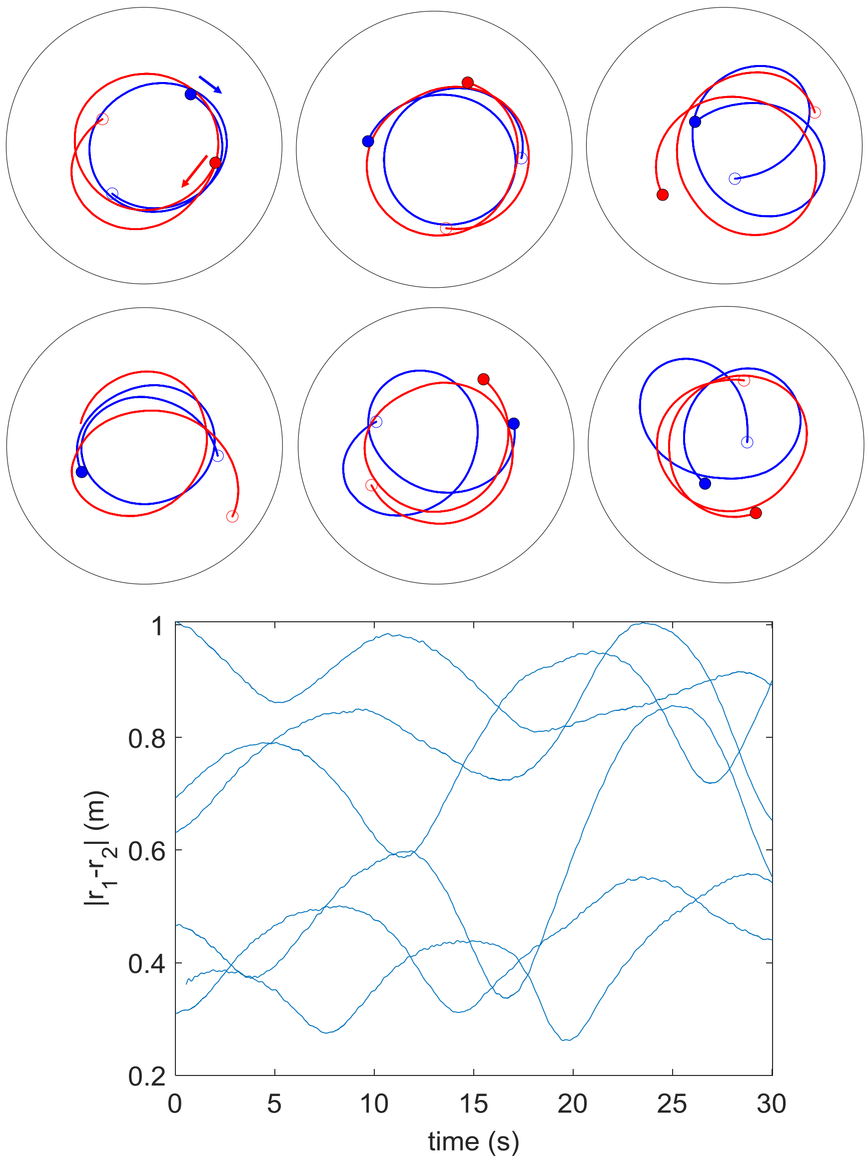

Figure S9: Dynamics of two vehicles with the same mass (a) Trajectories of vehicles with the same mass started at different initial conditions. (b) The relative distance of the two vehicles in (a).

S9. Supplementary movies

Movie S1: Trajectory of the heavy car (200 gr.) moving on elastic membrane: Circular orbit

A typical circular orbit: A video of a robotic vehicle driving on an elastic membrane with a central depression of 9.6 cm. Instantaneous velocity and radius (r) are marked with red and green arrows, respectively. The heading angle is the angle between the velocity and radius.

Movie S2: Trajectory of the heavy car (200 gr.) moving on elastic membrane: Retrograde precessing orbit

A typical precessing orbit (retrograde): A video of a robotic vehicle driving on an elastic membrane with a central depression of 9.6 cm. Instantaneous velocity and radius (r) are marked with red and green arrows, respectively. The tracking shows that the apsis of the orbit is rotating in the opposite direction of the orbit.

Movie S3: Trajectory of the light car (45 gr.) moving on elastic membrane: Prograde precessing orbit

A typical precession orbit (prograde): The lighter vehicle's orbit undergoes a prograde precession, i.e. the vehicle and the periapsis rotate clockwise. The mass of the vehicle is about one quarter the mass of the vehicle used in Movie S1 and S2. As predicted by the theory, a radial attraction $k(r)$ decreasing with r enabled by a lighter vehicle leads to the precession with the same sign of orbit, as opposed to the precession in Movie S2.

Movie S4: Deformation-only induced motion

In this movie, the membrane deformation is created by a human-controlled meter stick. The motion of the vehicle re-oriented by this deformation shows the deformation itself can act as a force to affect the motion of an object on the membrane.

Movie S5: Deformation-induced merger

In the first part, both panels show the trajectories of two vehicles moving on the membrane at the same time. The comparison is made regarding the mass ratio between the two vehicles: when the leading vehicle is heavy enough ($m_{21} = 1.37$), the two vehicles eventually merge while the $m_{21} = 1.00$ fails to merge. In the second part, the video on the right panel shows the virtual superimposition of independent runs of the two vehicles with the same mass ratio as the left panel shows that the substrate-mediated interaction is indeed making the two vehicles interact.

Movie S6: Controlling speed with tilt angle to avoid collisions

Each video shows the trajectories of the IMU-controlled vehicle (white chassis, solid line) and uncontrolled vehicle (gray chassis, dashed line) when a particular control magnitude $A = 0, 2, 4, 8$ is used.

Movie S7: Controlling speed with tilt angle to avoid collisions (Simulations of 5 vehicles)

The movie shows the simulations of 5 vehicles moving on the same membrane as in experiments. Starting from the same initial condition, the vehicles applied with speed control scheme avoid from collisions while the ones without merge quickly. More details can be found in Fig.9 of the main text and the corresponding section.